

Systematic experimental exploration of bifurcations with non-invasive control

D.A.W. Barton

Department of Engineering Mathematics, University of Bristol,
Queen's Building, University Walk, Bristol, BS8 1TR, U.K.

J. Sieber

College of Engineering, Mathematics and Physical Sciences, University of Exeter, Exeter, EX4 4QF, U.K.

We present a general method for systematically investigating the dynamics and bifurcations of a physical nonlinear experiment. In particular, we show how the odd-number limitation inherent in a popular non-invasive control scheme, (Pyragas) time-delayed feedback control, can be overcome for experiments with periodic forcing. To demonstrate the use of our non-invasive control, we trace out experimentally the resonance surface of a nonlinear oscillator near the onset of instability, around two saddle-node bifurcations (folds) and a cusp bifurcation.

PACS numbers: 05.45.Gg, 45.80.+r, 02.30.Oz

Keywords: experimental bifurcation analysis, non-invasive control, odd-number limitation

Feedback control is not only of interest as a tool for system manipulation in the classical control engineering sense, but it can also be used for model verification and discovery, if one can ensure that it is *non-invasive*. Pyragas' time-delayed feedback (TDF) is a popular feedback control scheme that is automatically non-invasive [1]. It feeds a signal $u(t) = k^T[y(t) - y(t - T)]$ back into the experimental dynamical system, where y is some system output (possibly processed), k is a vector or matrix of control gains and T is an a-priori chosen time delay. If the time delay equals the period of a periodic orbit $y(t)$ ($t \in [0, T]$) of the uncontrolled dynamical system and the gains are such that the control is stabilizing, then the controlled system will also have the periodic orbit y , because the control input u vanishes for all time (that is, the control becomes non-invasive). However, the control has changed the stability of y , making it visible in the experiment.

While sometimes TDF (or its extended version [2]) is used for engineering purposes (suppression of period doublings leading to chaos [3]), non-invasiveness is not essential in these applications. TDF draws interest mostly in the scientific community because it enables experimenters to explore dynamical phenomena such as equilibria and periodic orbits of the original uncontrolled system regardless of their dynamical stability [4, 5].

Systematic studies that try to explore parameter space of the uncontrolled system and that use TDF to stabilize equilibria and periodic orbits non-invasively encounter a major difficulty: it is not known under which conditions one can find control gains k that successfully stabilize a periodic orbit [6]. This is in contrast to classical feedback control where one feeds $u(t) = k^T[y(t) - y_*(t)]$ with a pre-determined reference signal $y_*(t)$ back into the system. For classical feedback control it is known that, if y_* corresponds to an equilibrium or periodic orbit of the uncontrolled system then, under some genericity assumptions (controllability and observability), one can always locally stabilize the equilibrium or periodic orbit even if it has arbitrarily many unstable eigenvalues [7]. Experimental and theoretical studies have explored the limits of applicability of

TDF and restrictions on the gains due to instabilities caused by the TDF feedback term $k^T[y(t) - y(t - T)]$ [5, 8]. In particular, there are topological restrictions (the *odd-number limitation* [9]) which guarantee that TDF cannot possibly work in some cases. Unfortunately, one common scenario where it would be natural to use TDF is ruled out by the odd-number limitation: an equilibrium of an autonomous system or a periodic orbit of a periodically forced system in the vicinity of a system parameter setting where it makes a fold (called saddle-node bifurcation, see the black markers in Fig. 2 for a typical bifurcation diagram). We note that even the unstable controller proposed in [10] fails to stabilize uniformly near the fold.

In this paper, we demonstrate a simple alternative approach to explore bifurcation scenarios, including the unstable branches. The demonstration experiment is the forced nonlinear oscillator shown in Fig. 1, an electro-magnetic energy harvester [11, 12], mounted on a force-controlled electro-dynamic shaker.

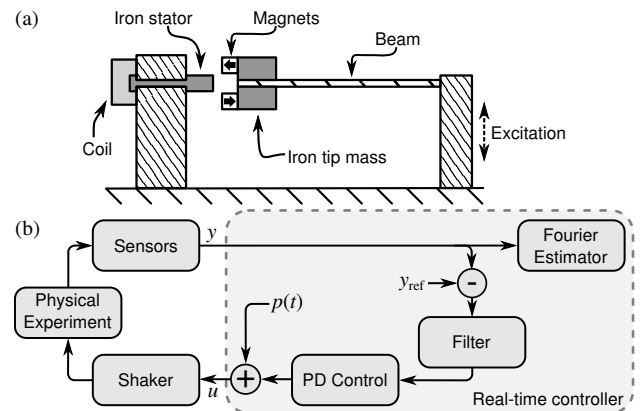


FIG. 1. (a) A schematic of the physical parts of the nonlinear energy harvester. (b) A schematic of the experimental set-up. The elements within the shaded box are implemented within a real-time control system. See [11] for implementation details.

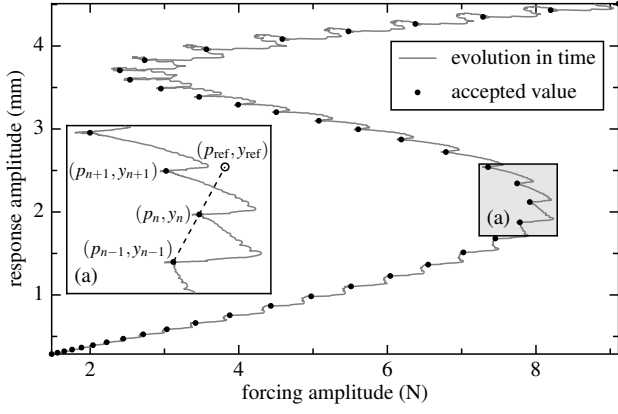


FIG. 2. Experimental data showing the evolution of the controlled system as the bifurcation diagram of the uncontrolled system (shown in Fig. 1(a)). A family of periodic orbits is tracked through two saddle-node bifurcations (folds). Artificially large steps are taken along the solution curve for illustration purposes. Forcing frequency: 22 Hz.

Our approach exploits the fact that the goal of the experiment is a parameter study in a system parameter p (in the set-up of Fig. 1, $p(t) = a \cos(\omega t)$, so we have two parameters), rather than finding a single equilibrium or periodic orbit at a specified parameter value. It is applicable whenever the feedback control is achieved by (effectively) varying the same system parameter p that one wants to use for the bifurcation diagram. We explain the basic principle first for equilibria, as illustrated by the inset (a) in Fig. 2 (the underlying data comes from the experiment, which is a harmonically forced oscillator, and requires a small modification of the basic principle, discussed afterwards).

Suppose we have an experiment with a single system parameter p (which we can vary) and a single output y , and we know that the feedback control law $u(t) = p_* + k[y_* - y]$ (control gain $k \neq 0$) is stabilizing the output y_* at parameter value p_* for all (p_*, y_*) along a branch of equilibria. Assume also that we have found already two previous points along the branch of equilibria, (p_{n-1}, y_{n-1}) and (p_n, y_n) (labeled by circular markers in Fig. 2(a)). We set

$$(p_{ref}, y_{ref}) = (p_n, y_n) + h[(p_n, y_n) - (p_{n-1}, y_{n-1})] \quad (1)$$

($h = 1$ in Fig. 2(a)), and run the experiment with control law

$$u(t) = p_{ref} + k[y_{ref} - y(t)]. \quad (2)$$

The experiment will settle asymptotically to a constant output value y_{asy} , which we call y_{n+1} , and a constant input value $u_{asy} = p_{ref} + k[y_{ref} - y_{asy}]$, which we call p_{n+1} , such that the new point along the branch is (p_{n+1}, y_{n+1}) . Only the combined parameter $Y_{ref} = p_{ref}/k + y_{ref}$ is varied during the experiment at discrete times. After each change of Y_{ref} and some transient time, the asymptotic values of the inputs and outputs give the parameters p_{n+1} and the output values y_{n+1} . In Fig. 2 two phases of the transients are visible between the black markers: the horizontal coordinate p can be set, so there is an initial sharp increase of p , followed by a gradual stabilization due to the control toward (p_{n+1}, y_{n+1}) .

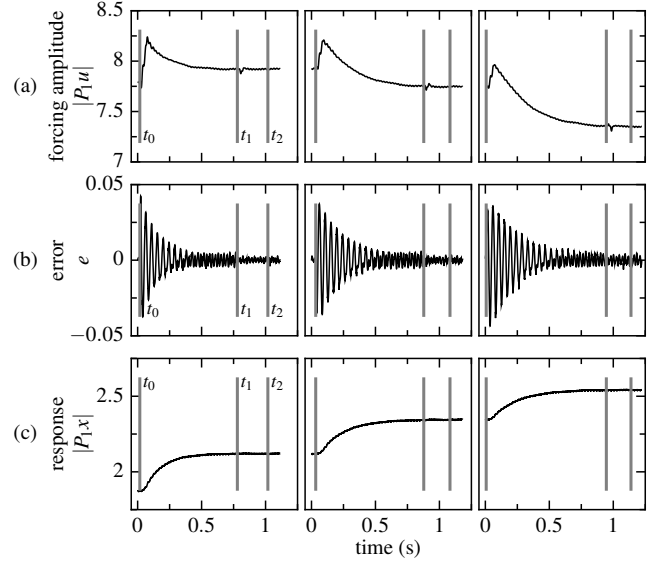


FIG. 3. Time profile of forcing and response amplitudes and error (non-harmonic part of control input u). Snapshots are time profiles corresponding to inset (a) of Fig. 2. Note that the time gaps between the time profiles are only gaps in the time series recordings due to the saving of data (typically of the order of milli-seconds); the experiment ran continuously. Forcing frequency: 22 Hz, sampling frequency: 5 kHz.

The approach illustrated in Fig. 2 should be compared to the general approach of solving the nonlinear fixed point problem

$$y_{ref} = y_{asy}(p_{ref}, y_{ref}), \quad (3)$$

in combination with a pseudo-arclength condition using a Newton iteration, introduced in [13]. The brackets in (3) indicate that the asymptotic output y_{asy} depends locally uniquely on parameter and reference signal if the feedback is stabilizing.

The method promises a substantial speed-up compared to [12, 13] by removing one equation per free bifurcation parameter from the fixed point problem, instead of adding an equation as is typically the case. The projection onto the solution surface occurs along the line $\{(p, y) : p = p_{ref} + k[y_{ref} - y]\}$ determined by the control gains k . Whenever the remaining equations of (3) can be solved by a fixed-point iteration (or there are no equations remaining), this removes the need for a full Newton iteration.

When the basic idea above is adapted to the scenario of a harmonically forced oscillator (where the bifurcation parameter is the forcing amplitude) the combined parameter $Y = p + k y_{ref}$ becomes time-dependent (periodic with the forcing period $2\pi/\omega$). One can still apply feedback law (2) using (p_{ref}, y_{ref}) defined by (1), and the input $u(t)$ will converge to a function $u_{asy}(t)$ asymptotically. However, u_{asy} will not be harmonic because the asymptotic output $y_{asy}(t)$ is not harmonic for a nonlinear oscillator. In this case, we can remove the higher harmonics using an iteration: define $P_k x$ as the k th (complex) Fourier coefficient of a periodic signal x , such that $x(t) = \sum_{k=0}^{\infty} \text{Re}[P_k x e^{ik\omega t}]$. Then we iterate the reference signals $Y_{ref} =$

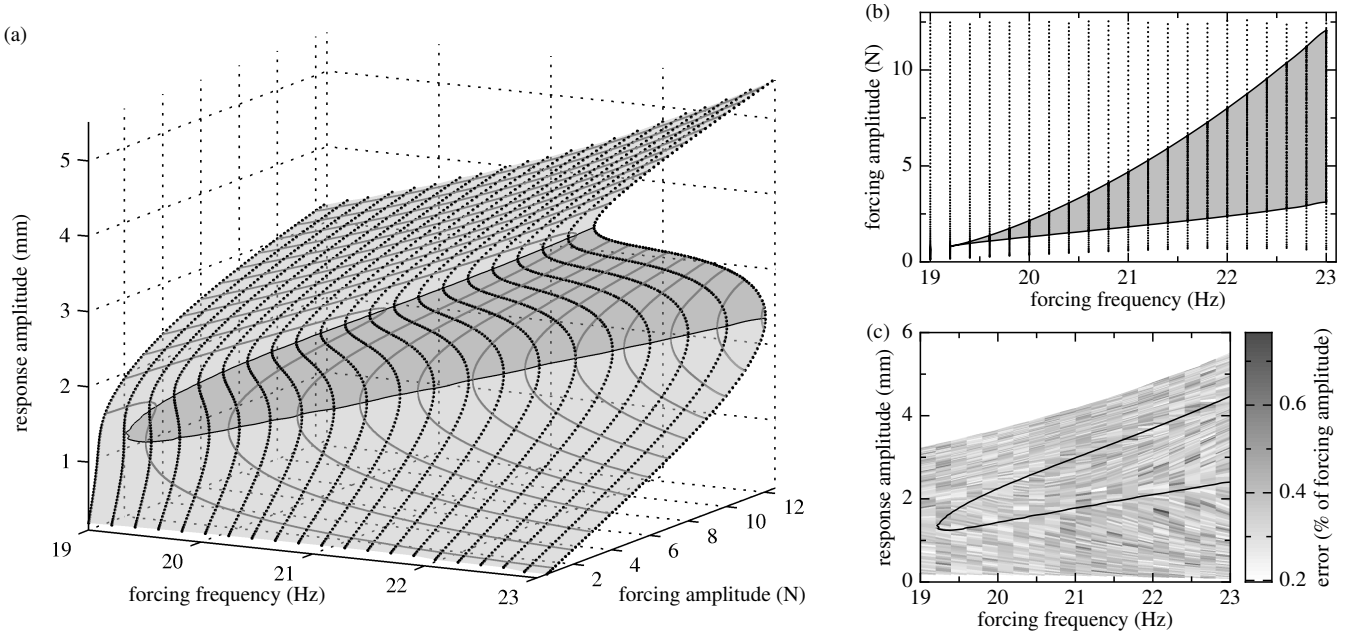


FIG. 4. Experimental results from the energy harvester shown in Fig. 1. A sequence of constant forcing frequency runs were performed at a spacing of 0.2 Hz. Panel (a) shows the complete resonance surface of the oscillator. Panel (b) shows the corresponding two-parameter bifurcation diagram (a top-down view of panel (a)) with the cusp point evident at approximately 19.2 Hz. Panel (c) is a front view of the resonance surface with the measured error superimposed onto the surface. The error is defined as the root-mean-square (RMS) difference between $u(t)$ and $p(t)$ as a percentage of the forcing amplitude; it measures how invasive the method is. In all panels, the data points are shown as black dots and the calculated saddle-node bifurcation (fold) curve is marked in black. Points within the dark gray region of panels (a) and (b) are unstable solutions.

$p_{\text{ref}}/k + y_{\text{ref}}$ in a Picard iteration:

$$Y_{\text{ref},0}(t) = Y_n(t) + h[Y_n(t) - Y_{n-1}(t)] \quad (4)$$

$$Y_{\text{ref},j+1}(t) = \text{Re}[P_1(Y_{\text{ref},j} - y_{\text{asy},j})e^{i\omega t}] + y_{\text{asy},j}(t), \quad (5)$$

where $y_{\text{asy},j}(t)$ is the asymptotic output signal for reference signal $Y_{\text{ref},j}(t)$. That is, the non-harmonic part of the next reference signal $Y_{\text{ref},j+1}$ is set to the non-harmonic part of the asymptotic signal of the output $y_{\text{asy},j}(t)$, and the harmonic part is kept constant for iterations $j \geq 1$.

In the experiment shown in Fig. 1, the non-harmonic parts of u_{asy} can be removed (to experimental accuracy) in a single iteration for all parameter values considered (see Fig. 3 and Fig. 4(c)). Thus, the overall protocol to find points along the solution branch is as follows.

1. Set $Y_{\text{ref},0}(t) = Y_n(t) + h[Y_n(t) - Y_{n-1}(t)]$.
2. Run the experiment with control law $u(t) = \text{PD}(y(t) - Y_{\text{ref},0}(t))$ until transients have settled, then record the asymptotic output $y_{\text{asy},0}(t)$.
3. Set $Y_{\text{ref},1}(t) = \text{Re}[P_1(Y_{\text{ref},0} - y_{\text{asy},0})e^{i\omega t}] + y_{\text{asy},0}(t)$,
4. Run the experiment with control law $u(t) = \text{PD}(y(t) - Y_{\text{ref},1}(t))$ until transients have settled, then record the asymptotic input $u_{\text{asy},1}(t)$ and output $y_{\text{asy},1}(t)$.

The next point on the branch is then $(p_{n+1}(t), y_{n+1}(t)) = (u_{\text{asy},1}(t), y_{\text{asy},1}(t))$, where $p_{n+1}(t)$ is harmonic up to experimental accuracy and $y_{\text{asy},1}(t)$ is the asymptotic output of the experiment in step 4. Note that the Fourier decomposition of u and y does not need to be done in real-time and instead can

be done as a post-processing step to choose the new reference signal $Y_{\text{ref},1}$ and to check convergence.

Figure 3 shows the time series recordings corresponding to the data points shown in Fig. 2(a); they demonstrate in detail the convergence of the method as the system passes through a saddle-node bifurcation (fold). The first harmonic of the input $P_1 u$ (Fig. 3(a)) gradually drifts during non-periodic transients but rapidly settles. The error $e(t) = u(t) - P_1 u e^{i\omega t}$ (Fig. 3(b)) corresponds to the non-harmonic, invasive, part of the control; its decay during each step is evident. The vertical bars (marked t_0 , t_1 and t_2) indicate the stages of the iteration: step 2 occurs from t_0 to t_1 , and step 4 occurs from t_1 to t_2 . The input u and output y at t_2 are then accepted as points on the branch when their corresponding Fourier coefficients become stationary for 5 consecutive forcing periods. Figure 3(c) shows the amplitude of the first harmonic $P_1 x$ of the displacement to further demonstrate convergence.

The main advantage of the method presented here over methods based on Newton iterations, apart from ease of implementation, is the speed-up of a factor of ≈ 15 compared to [12, 13] (a conservative estimate; only individual solution curves could be traced out in [12, 13]). This feature is particularly important if one wants to explore systems that gradually degrade under laboratory conditions.

As illustrated in Fig. 4(a), this speed-up enables tracking of entire surfaces and the associated bifurcations. The experimental data points (marked by black dots in panels (a) and (b)) are obtained by consecutive runs for fixed frequencies

0.2 Hz apart. The total experimental time to generate these results was 61 minutes. Panel (a) shows the three-dimensional projection in the space spanned by the two parameters forcing frequency and amplitude and the response amplitude (note that the response is non-harmonic and so this is indeed only a projection). Its main feature is the curve of saddle-node bifurcations passing through a cusp bifurcation (black) [14, 15]. Curves of constant forcing amplitude (gray), reminiscent of the resonance curves for an idealized Duffing oscillator, give additional geometric information. All the data points within the dark gray shaded area of Fig. 4(a) are unstable periodic orbits of the uncontrolled system, and as such would typically not be seen experimentally.

Figure 4(b) shows a top-down view of panel (a), a two-parameter bifurcation diagram, again indicating all measured points on the unstable part of the surface in a darker shade of gray. The saddle-node bifurcation (fold) curve bounds the instability region with a cusp point at approximately 19.2 Hz.

Figure 4(c) shows a front view of panel (a) with the error at each data point rendered onto the surface. Here the error is defined as the root-mean-square (RMS) difference between the actual input signal $u(t)$ (as fed into the shaker) and the reported harmonic forcing signal $p(t)$ (the harmonic part of u) as a percentage of the forcing amplitude. In essence, this is a measure of the invasiveness of the control; if this method was truly non-invasive, then this error would be zero. In the experimental set-up here the error is low, with a mean error of $< 0.5\%$. The predominant source of error is noise amplification through the use of a derivative controller. This error is kept to a minimum through the use of an appropriate digital filter [11]. As seen in Fig. 4(c), there is no apparent correlation between geometric features of the solution surface (e.g., the fold points) and the magnitude of the error at that point.

The presented approach is a general method to explore dynamical systems in parameter studies near saddle-node bifurcations (folds). It is particularly useful for the exploration of families of equilibria because no iterations similar to (5) are necessary. As we demonstrated, it is also applicable to periodically forced systems (the generalization to a non-harmonic forcing is straightforward). The main limitation of the method is that control fails at the linear level whenever the system does not depend on the bifurcation parameter to first order (e.g., near transcritical bifurcations). As the presented approach works particularly well around saddle-nodes, its main application areas are likely complementary to those of Pyragas control. Examples currently under investigation include the identification of growth rates in chemostats [16], or tracking localized spots in ferrofluids [17]

Acknowledgements: The research of J.S. is supported by EPSRC Grant EP/J010820/1.

- [2] J. E. S. Socolar, D. W. Sukow, and D. J. Gauthier, *Phys. Rev. E* **50**, 3245 (1994).
- [3] K. Yamasue, K. Kobayashi, H. Yamada, K. Matsushige, and T. Hikiyama, *Physics Letters A* **373**, 3140 (2009); A. Ahlborn and U. Parlitz, *Phys. Rev. Lett.* **93**, 264101 (2004).
- [4] M. Kim, M. Bertram, M. Pollmann, A. v. Oertzen, A. S. Mikhailov, H. H. Rotermund, and G. Ertl, *Science* **292**, 1357 (2001); S. Schikora, H.-J. Wünsche, and F. Henneberger, *Phys. Rev. E* **83**, 026203 (2011); S. Schikora, P. Hövel, H.-J. Wünsche, E. Schöll, and F. Henneberger, *Phys. Rev. Lett.* **97**, 213902 (2006); O. Lüthje, S. Wolff, and G. Pfister, *ibid.* **86**, 1745 (2001); D. J. Christini, J. J. Collins, and P. S. Lindsay, *Phys. Rev. E* **54**, 4824 (1996).
- [5] C. von Loewenich, H. Benner, and W. Just, *Phys. Rev. E* **82**, 036204 (2010).
- [6] E. Schöll and H. G. Schuster, eds., *Handbook of Chaos Control*, 2nd ed. (Wiley, New York, 2007).
- [7] E. D. Sontag, *Mathematical Control Theory: Deterministic Finite Dimensional Systems*, Texts in Applied Mathematics (Springer, 1998).
- [8] B. Fiedler, V. Flunkert, P. Hövel, and E. Schöll, *The European Physical Journal - Special Topics* **191**, 53 (2010); V. Flunkert and E. Schöll, *Phys. Rev. E* **84**, 016214 (2011); B. Fiedler, V. Flunkert, M. Georgi, P. Hövel, and E. Schöll, *Phys. Rev. Lett.* **98**, 114101 (2007).
- [9] H. Nakajima, *Phys. Lett. A* **327**, 44 (2004); E. W. Hooton and A. Amann, <http://arxiv.org/abs/1109.1138> (2011).
- [10] A. Tamasevicius, G. Mykolaitis, V. Pyragas, and K. Pyragas, *Phys. Rev. E* **76**, 026203 (2007).
- [11] The experimental set-up consisted of a generic electrodynamic shaker, a Maxon ADS 50/10 current controller and a dSpace DS1104 real-time measurement and control system. Displacement measurements were taken from the energy harvester using a suitably calibrated strain gauge. The real-time controller implemented a fourth order IIR Butterworth filter (-3 dB cut-off at 75 Hz) and a proportional-derivative controller. The derivative was estimated on-line using a two point finite difference. The filter was purely for the purposes of control; all other calculations used the unfiltered data. For the PD control $k_p x + k_d \dot{x}$, the control gains k_p and k_d were kept constant throughout. The Fourier coefficients were estimated in real-time using a recursive estimator to minimize discretization effects.
- [12] D. A. W. Barton, B. P. Mann, and S. G. Burrow, *Journal of Vibration and Control* **18**, 509 (2012); D. A. W. Barton and S. G. Burrow, *ASME Journal of Computational and Nonlinear Dynamics* **6**, 011010 (2011).
- [13] J. Sieber and B. Krauskopf, *Nonlinear Dynamics* **51**, 365 (2008); J. Sieber, A. Gonzalez-Buelga, S. A. Neild, D. J. Wagg, and B. Krauskopf, *Phys. Rev. Lett.* **100**, 244101 (2008).
- [14] To facilitate the extraction of geometric information, the data points in Fig. 4 are interpolated using Wendland's compactly supported radial basis functions [15, Ch. 11]. Using the interpolant, the bifurcation and constant forcing amplitude curves in Fig. 4(a,b) are calculated using numerical continuation.
- [15] G. E. Fasshauer, *Meshfree approximation methods with MATLAB* (World Scientific, 2007).
- [16] A. J. Veraart, E. J. Faassen, V. Dakos, E. H. van Nes, M. Lurling, and M. Scheffer, *Nature* **481** (2012); A. Rapaport, J. Sieber, S. Rodrigues, and M. Desroches, *Bioprocess and Biosystems Engineering* (submitted).
- [17] C. Gollwitzer, I. Rehberg, and R. Richter, *New Journal of Physics* **12**, 093037 (2010).